JGR Solid Earth

Key Points:

- We compare SHmax estimates derived from boreholes and from inversion of earthquake focal mechanisms to infer crustal stress heterogeneity
- Stress orientation varies with depth within sediment basins, but approaches more homogeneous basement orientations at bedrock interface
- Lateral stress orientation heterogeneity is mostly associated with basin margins and proximity to active faults at length scales of 1–20 km

Supporting Information:

- Supporting Information S1

Correspondence to:

K. Luttrell,
kluttrell@lsu.edu

A Unified Model of Crustal Stress Heterogeneity From Borehole Breakouts and Earthquake Focal Mechanisms

Karen Luttrell[1] [ID] **, and Jeanne Hardebeck[2]** [ID]

[1]Louisiana State University, Baton Rouge, LA, USA, [2]U.S. Geological Survey, Moffett Field, CA, USA

Abstract Observations of crustal stress orientation from the regional inversion of earthquake focal mechanisms often conflict with those from borehole breakouts, possibly indicating local stress heterogeneity, either laterally or with depth. To investigate this heterogeneity, we compiled SHmax estimates from previous studies for 57 near-vertical boreholes with measured breakout azimuths across the Los Angeles region. We identified subsets of earthquake focal mechanisms from established earthquake catalogs centered around each borehole with various criteria for maximum depth and maximum lateral distance from the borehole. Each subset was independently inverted for 3-D stress orientation and corresponding SHmax probability distributions, then compared with the corresponding borehole breakout-derived estimate. We find good agreement when both methods sample the basement stress (breakouts are close to the sediment-basement interface), or when both methods sample the mid-basin stress (sufficient earthquakes are present within a sedimentary basin). Along sedimentary basin margins, in contrast, we find acceptable agreement only when focal mechanisms are limited to shallow and close earthquakes, implying short-length-scale heterogeneity of <20 km. While the region as a whole shows evidence of both lateral and vertical stress orientation heterogeneity, we find a more homogeneous stress state within basement rock, over length scales of 1–35 km. These results reconcile the apparently conflicting observations of short-length-scale heterogeneity observed in boreholes, which sample primarily the basins, with the relative homogeneity of stress inferred from focal mechanisms, which sample primarily the basement, and imply distinct regimes for the appropriate use of each type of stress indicator.

Plain Language Summary Earthquakes and other tectonic phenomena respond largely to the state of stress within the Earth's crust, but this stress state is extraordinarily difficult to measure. Two methods are commonly used to estimate at least the orientation of the stress field within the crust: the azimuth of breakout fractures observed within drilled boreholes, which tend to be <3 km deep within sedimentary basins, and the inversion of sets of earthquake focal mechanisms observed seismically, which tend to be >5 km deep within bedrock. Studies using these two techniques have repeatedly arrived at different conclusions about how variable the crustal stress field is, and particularly have disagreed about the distances over which those variations occur. The discrepancy may be due to differences in the volume of crust sampled by each estimate, and we test this by systematically comparing observations from both types of estimates using a range of different crustal volumes. We find that if the two estimates are made near enough to one another, especially in depth, they generally agree, but "how near is near enough" changes depending on the local geology. These investigations help bridge the gap between our understanding of how stress changes over different length scales.

1. Introduction

The crustal stress field plays an important role in understanding earthquake processes and predicting ground motions from earthquakes (Harris et al., 2018), but direct observation of stress state is difficult (Zoback et al., 2010). Observations of stress field orientation may be provided either by the inversion of earthquake focal mechanisms (FMs) (Hardebeck & Hauksson, 2001; Hardebeck & Michael, 2006; Michael, 1984, 1987; Yang & Hauksson, 2013) or by the azimuth of borehole breakouts (BH) (Kerkela & Stock, 1996; Mount & Suppe, 1992; Shamir & Zoback, 1992; Stock & Healy, 1988; Wilde & Stock, 1997; Zajac & Stock, 1997; Zoback & Healy, 1992). However studies of these stress indicators have reached different conclusions about the extent and characteristic length scales of heterogeneity in areas of active faulting, with studies
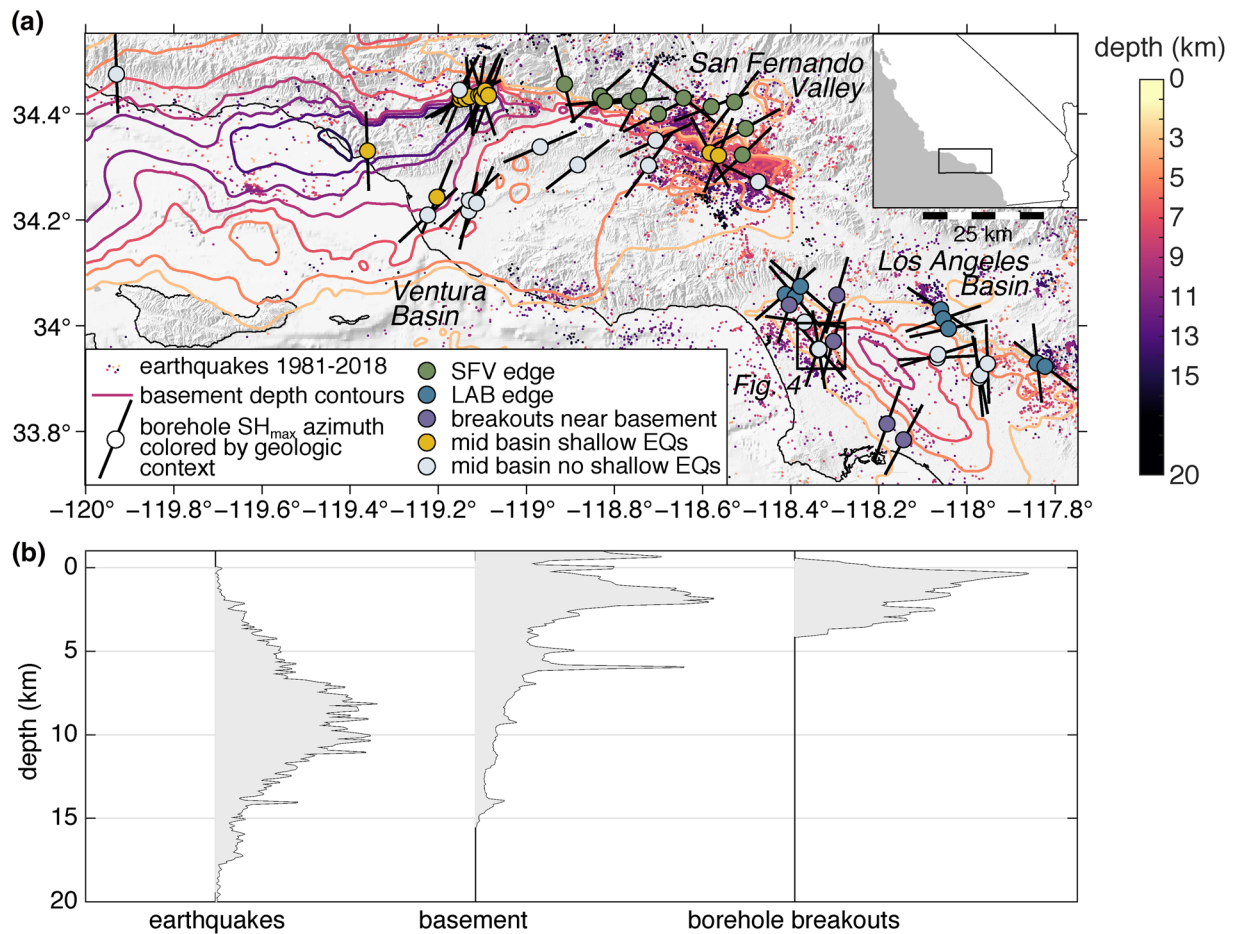
Figure 1. (a) map of boreholes considered in this study (Table 1), colored by geologic context, with estimates of SHmax azimuth from breakouts indicated by thick black lines. Contours of depth to sediment basement interface (Shaw et al., 2015) for 3–15 km depth are shown as thick colored lines. Dots indicate earthquakes with available focal mechanism solutions (Yang et al., 2012), colored by depth. (b) Depth distributions of earthquakes, sediment-basement interface, and breakout ranges in the boreholes considered.

of predominantly FMs finding smooth variations at regional length scales of tens to hundreds of kilometer (Heidbach et al., 2018; Yang & Hauksson, 2013) and studies of BHs finding considerable heterogeneity at local length scales as low as 1 km (Schoenball & Davatzes, 2017; Wilde & Stock, 1997). This leaves researchers unclear about how to best represent the stress field at intermediate length scales of ~1–15 km (Harris et al., 2018).

The main difference between these two measurement types is the crustal volume represented by each. Near-vertical boreholes provide a direct observation of maximum horizontal compressional stress (SHmax) azimuth at a discrete location over the depth range of existing breakouts, which are typically within sedimentary basins. FM stress inversion requires a population of FMs derived from earthquake records, and the resulting 3-D stress orientation represents the entire crustal volume sampled by those earthquakes, which are predominantly within bedrock. The goal of this work is to test whether differences in either depth or volume sampled can account for the discrepancies in stress orientation indicated by the two techniques, and if so over what length scale that transition occurs. We use the Los Angeles area (Figure 1) as a natural laboratory because of the readily available BH and FM data, the complexity of the stress field in that region, and because of the practical importance of understanding the stress field in areas with high seismic hazard.

We identify 57 BHs with published SHmax estimates (Table 1) and perform new FM inversions for earthquake populations (Yang et al., 2012) covering a range of depth and distance criteria. We then interpret the variations in SHmax agreement over different crustal volumes sampled by FMs for indications of the spatial

Table 1
SHmax Estimates From Borehole Breakouts Used in This Study

BH #	Geologic context	Latitude[a]	Longitude[a]	Breakout depth range (m)	SHmax azimuth[b] (°EofN)	Reference
1	SFV edge	34.4558	−118.9133	124 – 159	166 ± 14	Wilde and Stock (1997)
2	SFV edge	34.4333	−118.8317	637 – 804	48 ± 4	Wilde and Stock (1997)
3	SFV edge	34.4242	−118.8215	893 – 906	84 ± 3	Wilde and Stock (1997)
4	SFV edge	34.4231	−118.7663	246 – 1,027	85 ± 11	Wilde and Stock (1997)
5	SFV edge	34.4333	−118.7448	635 – 866	28 ± 9	Wilde and Stock (1997)
6	SFV edge	34.4000	−118.7000	940 – 940	63 ± 0	Wilde and Stock (1997)
7	SFV edge	34.4300	−118.6428	1,356 – 3,624	128 ± 28	Mount and Suppe (1992)
8	SFV edge	34.4133	−118.5797	2,897 – 3,964	69 ± 22	Mount and Suppe (1992)
9	SFV edge	34.4219	−118.5281	1,995 – 2,331	38 ± 11	Mount and Suppe (1992)
10	SFV edge	34.3226	−118.5090	316 – 850	46 ± 0.3	Kerkela and Stock (1996)
11	SFV edge	34.3731	−118.5026	76 – 326	61 ± 0.3	Kerkela and Stock (1996)
12	LAB edge	34.0603	−118.4119	2,432 – 2,576	49 ± 7	Mount and Suppe (1992)
13	LAB edge	34.0554	−118.3902	2,440 – 2,657	140 ± 7	Wilde and Stock (1997)
14	LAB edge	34.0750	−118.3780	331 – 435	131 ± 0	Wilde and Stock (1997)
15	LAB edge	34.0308	−118.0600	1,566 – 1,890	124 ± 5	Wilde and Stock (1997)
16	LAB edge	34.0138	−118.0533	365 – 2,661	71 ± 19	Wilde and Stock (1997)
17	LAB edge	33.9946	−118.0420	358 – 797	78 ± 18	Wilde and Stock (1997)
18	LAB edge	33.9296	−117.8400	422 – 1,506	174 ± 20	Wilde and Stock (1997)
19	LAB edge	33.9238	−117.8221	283 – 1139	128 ± 12	Wilde and Stock (1997)
20	Breakouts near basement	34.0394	−118.4031	3,109 – 3,450	16 ± 9	Mount and Suppe (1992)
21	Breakouts near basement	33.9567	−118.3381	2,708 – 2,969	18 ± 4	Mount and Suppe (1992)
22	Breakouts near basement	33.9550	−118.3360	1,559 – 2,123	171 ± 13	Wilde and Stock (1997)
23	Breakouts near basement	33.9706	−118.3033	1,568 – 3,246	16 ± 19	Mount and Suppe (1992)
24	Breakouts near basement	34.0583	−118.2948	1,334 – 1,751	16 ± 8	Wilde and Stock (1997)
25	Breakouts near basement	33.8142	−118.1808	1,105 – 1,606	19 ± 25	Mount and Suppe (1992)
26	Breakouts near basement	33.7847	−118.1433	2,469 – 3,532	28 ± 28	Mount and Suppe (1992)
27	Mid basin shallow EQs	34.3297	−119.3608	3,530 – 4,185	178 ± 19	Mount and Suppe (1992)
28	Mid basin shallow EQs	34.2436	−119.2031	3,018 – 4,039	22 ± 24	Mount and Suppe (1992)
29	Mid basin shallow EQs	34.4278	−119.1508	1,205 – 1,443	61 ± 5	Mount and Suppe (1992)
30	Mid basin shallow EQs	34.4337	−119.1483	2,570 – 2,663	22 ± 3	Wilde and Stock (1997)
31	Mid basin shallow EQs	34.4281	−119.1375	918 – 1,049	62 ± 8	Mount and Suppe (1992)
32	Mid basin shallow EQs	34.4329	−119.1285	175 – 226	175 ± 18	Wilde and Stock (1997)
33	Mid basin shallow EQs	34.4343	−119.1084	480 – 546	9 ± 9	Wilde and Stock (1997)
34	Mid basin shallow EQs	34.4366	−119.1023	740 – 751	24 ± 2	Wilde and Stock (1997)
35	Mid basin shallow EQs	34.4304	−119.0988	869 – 1,829	162 ± 9	Wilde and Stock (1997)
36	Mid basin shallow EQs	34.4438	−119.0937	2,494 – 2,545	22 ± 4	Wilde and Stock (1997)
37	Mid basin shallow EQs	34.4342	−119.0850	557 – 1,024	20 ± 3	Wilde and Stock (1997)
38	Mid basin shallow EQs	34.3272	−118.5833	505 – 1,892	152 ± 8	Wilde and Stock (1997)
39	Mid basin shallow EQs	34.3220	−118.5637	1,401 – 2,994	21 ± 0.3	Kerkela and Stock (1996)
40	Mid basin no shallow EQs	34.4750	−119.9300	284 – 558	178 ± 12	Wilde and Stock (1997)
41	Mid basin no shallow EQs	34.2092	−119.2230	2,439 – 3,605	47 ± 21	Wilde and Stock (1997)
42	Mid basin no shallow EQs	34.4453	−119.1514	2,595 – 2,745	29 ± 17	Mount and Suppe (1992)
43	Mid basin no shallow EQs	34.2175	−119.1311	2,035 – 2,882	13 ± 9	Mount and Suppe (1992)

Table 1
Continued

BH #	Geologic context	Latitude[a]	Longitude[a]	Breakout depth range (m)	SHmax azimuth[b] (°EofN)	Reference
44	Mid basin no shallow EQs	34.2368	−119.1292	2,467 – 2,510	48 ± 42	Wilde and Stock (1997)
45	Mid basin no shallow EQs	34.2325	−119.1125	2,292 – 2,683	24 ± 2	Mount and Suppe (1992)
46	Mid basin no shallow EQs	34.3378	−118.9681	412 – 1,815	67 ± 15	Mount and Suppe (1992)
47	Mid basin no shallow EQs	34.3042	−118.8833	1,605 – 2,209	52 ± 11	Wilde and Stock (1997)
48	Mid basin no shallow EQs	34.3035	−118.7225	155 – 687	36 ± 11	Wilde and Stock (1997)
49	Mid basin no shallow EQs	34.3500	−118.7063	200 – 282	65 ± 19	Wilde and Stock (1997)
50	Mid basin no shallow EQs	34.2718	−118.4737	73 – 2,256	116 ± 0.3	Kerkela and Stock (1996)
51	Mid basin no shallow EQs	34.0080	−118.3683	568 – 604	98 ± 5	Wilde and Stock (1997)
52	Mid basin no shallow EQs	33.9560	−118.3350	147 – 215	139 ± 8	Wilde and Stock (1997)
53	Mid basin no shallow EQs	33.9400	−118.0667	387 – 504	87 ± 19	Wilde and Stock (1997)
54	Mid basin no shallow EQs	33.9457	−118.0650	397 – 1,250	73 ± 11	Wilde and Stock (1997)
55	Mid basin no shallow EQs	33.9029	−117.9733	1,136 – 1,136	174 ± 0	Wilde and Stock (1997)
56	Mid basin no shallow EQs	33.9075	−117.9698	1,046 – 1,236	169 ± 4	Wilde and Stock (1997)
57	Mid basin no shallow EQs	33.9281	−117.9531	1,020 – 1,242	178 ± 6	Mount and Suppe (1992)

[a]Reported locations have uncertainty of ≤1 km. [b]Reported standard deviation of observed breakouts listed, effective uncertainty is the larger of reported standard deviation or 10°.

variability in stress state heterogeneity. If the stress field is relatively homogeneous within the volume sampled by the BH and FMs, we would expect good agreement in SHmax orientation. If the stress field is more heterogeneous, we would expect the agreement in SHmax orientation to improve the more closely the FMs are located to the borehole breakouts. In particular, if stress or stress heterogeneity varies with depth, or differs between basin and bedrock, we would expect the agreement to improve the closer in the depth the FMs are to the breakout depth.

Borehole observations are not uniformly distributed across the Los Angeles region. They tend to be derived from wells drilled for oil and gas exploration, and as such are biased toward areas with thicker sediment cover, including the Los Angeles, San Fernando, and Ventura basins. Figure 1b shows depth histograms of seismicity (Yang et al., 2012), sediment-basement interface (Shaw et al., 2015), and available borehole breakouts (Table 1). While BHs are mostly shallow and FMs mostly deeper, there is some overlap in the 3–5 km range, which coincides with basin depths across much of the region. We therefore interpret stress orientation heterogeneity not only across the entire region but also according to the geologic context of each BH relative to sediment basin structures. The results will be used to describe characteristic behaviors of stress orientation rotation across the region, with implications for stress heterogeneity in similar systems around the world.

2. Methods

2.1. Borehole Observations Compiled From Previous Studies

The most direct observations of the 3-D in situ stress field within the seismogenic crust come from drilling for scientific or industrial purposes, where a combination of borehole breakouts and hydraulic fracturing can be used to estimate the orientation of the stress field, and in some cases be used to estimate the full in situ stress tensor (e.g., Brudy et al., 1997; Hickman and Zoback, 2004; Kerkela & Stock, 1996; Mount & Suppe, 1992; Shamir & Zoback, 1992; Stock & Healy, 1988; Wilde & Stock, 1997; Zajac & Stock, 1997; Zoback and Healy, 1992; Zoback et al., 2010). If a borehole is near-vertical and one of the principal stress directions is near-vertical, then the azimuth of SHmax can be inferred to be 90° from the azimuth of the borehole breakouts (e.g., Plumb & Hickman, 1985). When a well is deviated, or none of the principal stress axes are near-vertical, then the relationship between SHmax azimuth and borehole breakout azimuth is less straightforward, but if enough breakouts are available in deviated boreholes of varying orientations within

an area, the three-dimensional stress orientation can in some cases be estimated (e.g., Mastin, 1988). In these ways, boreholes provide an opportunity to estimate stress state at a specific location within 3-D space with very little spatial averaging.

Wilde and Stock (1997) analyzed 4-arm oriented caliper data from 71 wells across southern California from Los Angeles to Santa Barbara, divided into six subregions, with the goal of both estimating the SHmax direction and constraining the stress regime across the subregions. We treat each borehole individually and exclude from consideration wells that are highly deviated (such that determination of SHmax direction is not straightforward), wells whose breakouts the authors determined were not reliable indicators of SHmax direction (e.g., key seats), and wells located outside the range of the Southern California Earthquake Data Center (SCEDC) catalog, leaving 35 wells for consideration. Mount and Suppe (1992) compiled 118 breakout azimuths from near-vertical (<10º deviation) wells across California, of which 18 are within both the range of the SCEDC catalog and the current study area. Kerkela and Stock (1996) analyzed data from 10 wells in the San Fernando Valley area, of which four were near-vertical (<5° deviation).

For the 57 individual wells we consider, the SHmax direction is inferred to be 90° from the observed breakout azimuth (Table 1). For each study, the uncertainty in breakout azimuth is calculated as the standard deviation of breakout azimuths observed within each borehole. However, this leads to artificially small uncertainties when data is sparse (e.g., a standard deviation of 0° when only one breakout is present within a well). We therefore adopt a functional uncertainty for each borehole that is the larger of either the stated standard deviation or the mean of all the stated standard deviations (10°). We also note that for many wells, the locations are specified only by Public Land Survey System township, range, and section, suggesting well locations should be considered to have an uncertainty of 1 km.

2.2. Inversion of Earthquake Focal Mechanism Subsets

For this analysis, we used the updated catalog of 216,000 earthquake focal mechanisms from 1981 to 2018 from the SCEDC (Yang et al., 2012), of which 21,000 are within our study area. The earthquakes in this catalog have absolute location errors of <1 km (Hauksson et al., 2012), so we consider their locations to be known more precisely than those of the BH. For each of the 57 boreholes listed in Table 1, we identified subsets of focal mechanisms that fit a certain maximum depth (z_{max}) and maximum lateral distance (d_{max}) criteria (Figure). We invert each subset of focal mechanisms for 3-D stress orientation using the method of Michael (1984), which minimizes the difference between the rake direction of each mechanism and the resolved shear stress on the fault plane. The nodal plane ambiguity is addressed by choosing the nodal plane with the greatest instability in the stress field, and the stress model and nodal plane are iterated until they stabilize (Vavryčuk, 2014). Uncertainty is determined using bootstrap resampling, with 1000 iterations (Michael, 1987). For each subset, we identify the SHmax orientation of the best stress tensor, and represent the uncertainty probability density function (PDF) of SHmax values with 5° resolution. While we invert for 3-D principal stress axes, we report only the predicted SHmax azimuths to compare directly with borehole observations.

Because our analysis is limited by the number of earthquakes available, we choose to use all focal mechanisms, regardless of quality. In testing, we found the increase in uncertainty associated with using "C" or "D" quality mechanisms were negligible relative to the increase in uncertainty associated with reducing the number of mechanisms used in each inversion. Theoretically, a stress tensor can be determined for a population of six or more individual focal mechanisms, but in practicality, well-constrained solutions require a population of at least 10 earthquakes. We identified 3 z_{max} (all depths, shallower than 5 km, shallower than 3 km) and 14 d_{max} (1–35 km) values, for a total of 2,394 individual stress inversions. In practice, not all boreholes have a sufficient number of earthquakes within a given depth or distance criteria to compute a valid stress estimate, so the actual number of inversions computed is 2,059.

2.3. Comparing Borehole and Focal Mechanism Data

We compare pairs of BH and FM SHmax estimates by calculating the absolute circular difference (ACD) $\in [0°, 90°]$, which emphasizes the degree of misfit independent of whether the FM SHmax estimate is clockwise or counterclockwise from the BH SHmax estimate. Confidence is expressed as the PDF of each ACD,
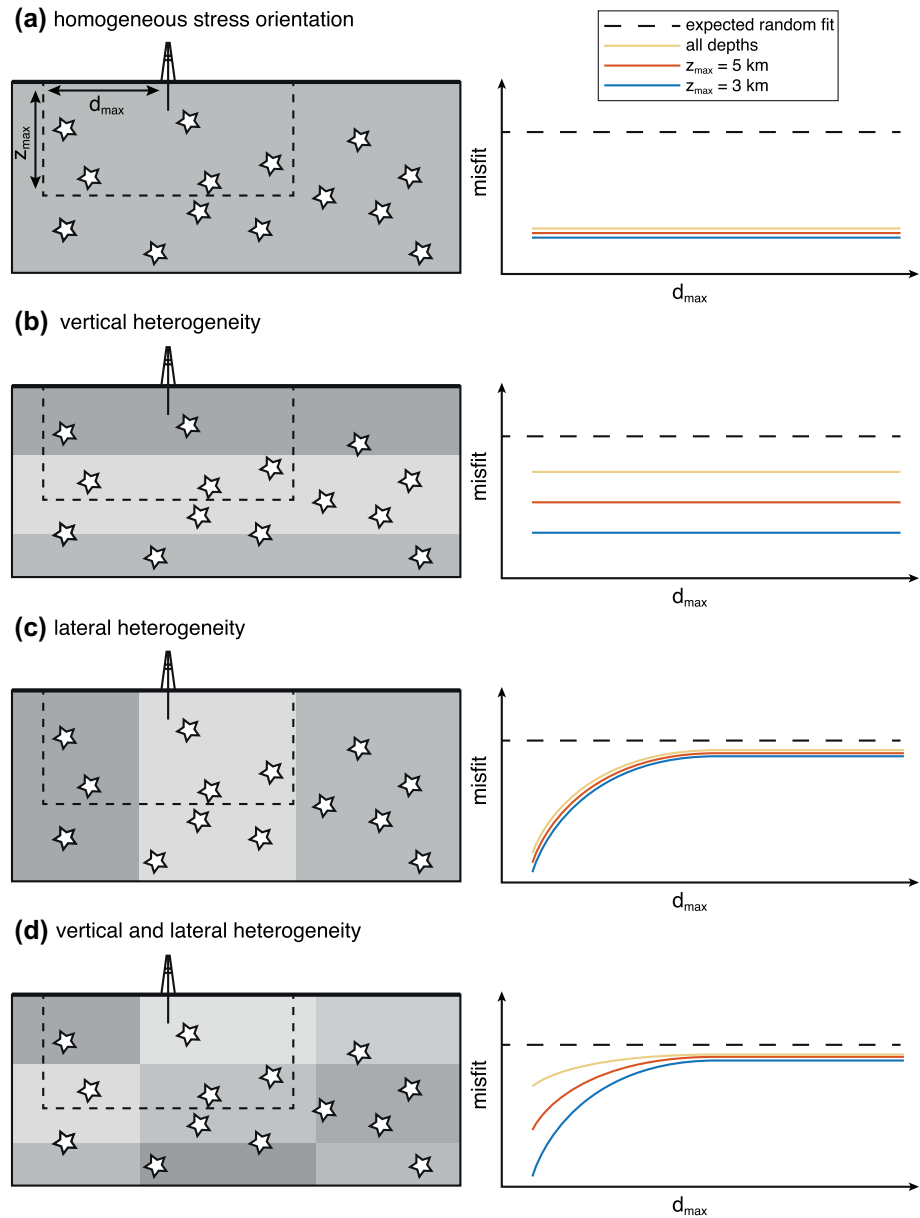
Figure 2. Schematic of possible stress orientation arrangements in the shallow crust, along with the expected behavior of FM versus BH misfit as a function of d_{max} and z_{max}. Stars represent earthquakes in the vicinity of the borehole. Only those within the cylinder range defined by d_{max} and z_{max} (dashed box) are considered for a given focal mechanism inversion. Expected shapes are shown for shallowest (blue), shallow (orange), and all depths (yellow) of earthquakes. Because ACD has a finite range, there is a certain level of misfit that would be expected even from uniformly distributed random azimuths (dashed line).

calculated assuming the BH SHmax PDFs are uniform on the interval of the SHmax estimate ± the effective SHmax uncertainty (Table 1). To characterize the SHmax misfit for a set of BH FM pairs, we calculate the root mean square (RMS) of the corresponding set of individual ACD values. For each population, an ACD RMS PDF is calculated from bootstrap resampling of the individual ACD PDFs using 10^6 samples. Because the range of possible SHmax values is bounded, there is a certain level of misfit that would be expected even if the SHmax azimuths were distributed randomly. For the RMS metric, this can be calculated analytically based on the expected value of the square of a random variable uniformly distributed on $\in \left[0°, 90° \right]$ as
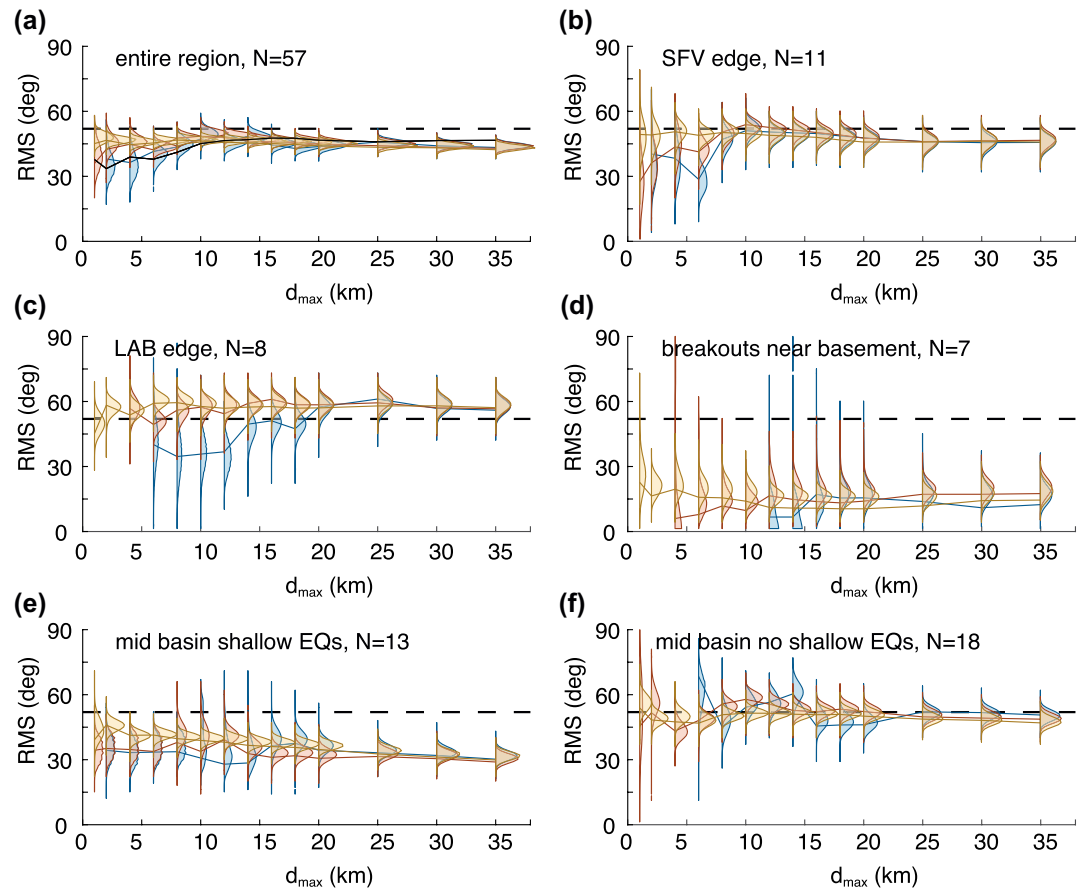
Figure 3. PDF distributions of ACD RMS for (a) all boreholes across entire region and (b)-(f) borehole subsets based on geologic context as indicated in Figure 1 and Table 1. Earthquake subsets using shallowest earthquakes with depth < 3 km (blue), shallow earthquakes with depth < 5 km (red), and all available earthquakes (yellow) shown. Dashed line represents expected random fit, and solid colored lines represent RMS using best estimate of borehole and focal mechanism SHmax. Solid black line in (a) represents ACD RMS between pairs of boreholes within the specified maximum distance. *N* indicates the number of boreholes included in each subgroup. ACD, absolute circular difference; RMS, root mean square.

$90° / \sqrt{3}$ = 51.96°. Any RMS at or above this level fits no better than random (dashed black line in Figures 2 and 3), so this can be used as one measure of significance.

2.4. Borehole Subgroups by Geologic Context

In order to test specific hypotheses about stress heterogeneity and the causes of discrepancy between BH and FM observations, it is instructive to consider both the overall ACD RMS results from the entire region and the ACD RMS from groups of boreholes sorted by their immediate geologic context rather than their geographic subregion. To this end, we divided the 57 boreholes into five categories (Figure 1 and Table 1), based on the spatial relationship between the boreholes, nearby earthquakes, and sediment-basement interface (Shaw et al., 2015). First, we identify 19 boreholes that occur near the edge of a sedimentary basin, generally close to an active fault bounding the basin and in sediments <4 km deep. Of these, 11 are on the north edge of the San Fernando Valley basin (green circles), in the vicinity of strands of the San Cayetano and Oak Ridge fault zones, while eight of them are along the north and northeast edges of the Los Angeles basin (dark blue circles), in the vicinity of the Whittier fault and Santa Monica thrust. Of those boreholes within a sedimentary basin, seven of them within the Los Angeles basin have breakouts that are within 3 km of the sediment-basement interface (purple circles). Of the remaining boreholes, 13 occur in regions

where at least 25% of the earthquakes within 10 lateral km occur above the sediment basement interface (yellow circles), and 18 occur in places without substantial earthquake activity within the sediments (light blue circles).

2.5. Expected Results for Multiple Working Hypotheses

In general, we move forward with four working hypotheses about possible stress orientation distribution, each of which would have a distinct pattern of borehole versus earthquake focal mechanism misfit as a function of d_{max} and z_{max} (Figure 2). If the stress state were homogeneous over depth and across areas up to the maximum d_{max} value considered (35 km), we would expect good agreement between the two SHmax estimates regardless of which subset of earthquakes were included in the focal mechanism inversion (Figure 2a). If there is vertical heterogeneity in stress orientation (Figure 2b), we expect FM SHmax values considering only the shallowest earthquakes (blue line) to fit better than those also considering deeper earthquakes (orange line) or those considering earthquakes of any depth (yellow line), independent of choice of d_{max}. If stress orientation heterogeneity is purely lateral (Figure 2c), we expect focal mechanism inversions involving only closer earthquakes (smaller d_{max} values) to fit better than those covering a larger area, but with no difference between earthquake subsets with different z_{max} values. If stress orientation is heterogeneous in both the vertical and lateral directions (Figure 2d), we expect misfit to generally improve for lower d_{max}, but we expect that improvement to be more pronounced for subsets involving only the shallowest earthquakes.

Our interpretation will necessarily be hampered by the uneven distribution of earthquakes throughout the crust. In particular, for each borehole considered, there may not be sufficient earthquakes at low d_{max} and z_{max} values to compute a valid stress state inversion. This would be equivalent to erasing the left ends of the orange and especially blue lines in Figure 2. Even so, we expect particular features of the misfit curves to offer further insight. In the case of lateral heterogeneity (Figure 2c or 2d), the d_{max} value at which misfit values start to decrease puts an upper limit on the length scale of lateral heterogeneity in the area. If misfit improves to within uncertainty, the d_{max} value at which RMS intersects zero provides a lower limit on the length scale of lateral heterogeneity. If the misfit curve remains significantly different from zero, it indicates that heterogeneity exists at scales smaller than those able to be considered by the available distribution of earthquakes.

3. Results

3.1. Results for Individual BHs and FM Inversions

Figures SA1–SA14 show the map view summary of best-fitting SHmax values derived from focal mechanism subsets satisfying various criteria, around each of the 57 boreholes across the study area. When considering all earthquakes within 35 km d_{max} from a borehole (Figure SA1), the resulting SHmax directions vary smoothly across the region from ~0–10°EofN. As the d_{max} values decrease, the resulting solutions increase in heterogeneity, but even at the smallest distances for which inversions can be calculated (Figure SA14), they do not appear to capture the full heterogeneity observed in the borehole SHmax values. Figures SB1–SB57 show the ACD PDFs between each individual borehole and the FM SHmax estimates for different earthquake subsets, numbered by the BH # listed in Table 1.

The borehole observations themselves exhibit varying degrees of heterogeneity (Figure 1) with some having relatively consistent SHmax azimuths (e.g., south Ventura Basin), others exhibiting bimodal distributions that are nearly orthogonal (north San Fernando Valley), and still others being almost uniformly distributed in azimuth (Los Angeles Basin). One should not expect the FM observations to fit the BH observations at a given distance better than the BH observations fit themselves. We therefore calculate the expected ACD RMS from pairs of boreholes that are a comparable distance apart, illustrated by the black line in Figure 3a. Borehole pairs greater than 10 km apart have an RMS misfit of ~45°, slightly better than random. For pairs less than 10 km apart, RMS misfit decreases gradually to ~35° for pairs <2 km apart.

3.2. Composite Results Across the Entire Region

Figure 3a shows the ACD RMS PDFs for all 57 boreholes considered (Figure 1), as a function of d_{max} and z_{max}. When earthquakes of all depths are considered (yellow), the overall misfit remains at $\sim 45°$ regardless of proximity to the individual borehole. This is better than would be expected if the SHmax estimates were distributed uniformly (dashed line), indicating some sensitivity to broad regional stress state, but also that proximity alone is insufficient to account for the observed discrepancies. When only shallow earthquakes ($z_{max} = 3$ km) are considered (blue), we see that when earthquakes beyond $\sim$10 km are included, the misfit remains constant at $\sim$45°. However, for $d_{max} < 10$ km, there is a gradual improvement in misfit to $\sim$35°. (Note the widening of the PDF due to the smaller number of boreholes with sufficient earthquakes satisfying these depth and distance criteria to compute a valid stress inversion solution.) While these RMS values represent a coarse level of agreement, they are on-par with the level of agreement observed between borehole pairs at these distances (black line). In that regard, it would be surprising if the focal mechanism solutions were able to fit the borehole SHmax observations better than the boreholes could fit themselves. With an intermediate z_{max} of 5 km, there is some improvement at distances of <10 km, but less so than observed when using only the shallowest 3 km. Overall this indicates substantial regional heterogeneity in the stress field (e.g., Figure 2d), both vertically and laterally at length scales <10 km.

3.3. Geologic Context Subset Results

Figures 3b–3f show the ACD RMS PDFs for the five geologic context subgroups (Figure 1 and Table 1 and Section 2.4). We find that boreholes within the sedimentary basin with breakouts close to the sediment-basin interface (Figure 3d) are consistently well fit to the earthquake-derived SHmax, within 20° RMS for any depth and distance criteria, and in many cases fitting to within uncertainty for solutions derived from the shallowest and closest focal mechanisms. This suggests that both methods are sampling an essentially homogeneous basement stress state (e.g., Figure 2a). Boreholes within a basin in regions where earthquakes are present within the sediments (Figure 3e) fit moderately well, with $\sim$35° RMS, while boreholes in regions without shallow earthquakes (Figure 3f) fit their focal mechanism counterparts no better than random. Neither of these cases demonstrate improvement when considering only shallower or closer sets of earthquakes. These results suggest a stress field that varies with depth (e.g., Figure 2b), particularly with a difference between the basin and the bedrock. The moderate fit between FM and BH that both sample the basin suggests that the stress within the basin is relatively homogeneous, although less so than the basement.

For boreholes along the edge of a basin (Figures 3b and 3c), both show a similar pattern in which sets of shallower and closer earthquakes fit significantly better than earthquakes of any depth or distance, which fit no better than random. In the case of the Los Angeles basin (Figure 3c), the shallowest earthquakes (depths < 3 km) within 20 km of the borehole, and especially within 12 km of the borehole, fit much better with RMS $\sim 35°$. For the San Fernando Valley (Figure 3b), we find that earthquakes within 10 km fit better, with steady improvement for shallow (depth < 5 km) and shallowest (depth < 3 km) subsets and RMS values as low as 25°. This suggests that the stress state near the basin edges varies both laterally and with depth (e.g., Figure 2d) in the transition between basin and bedrock stress states. The length scale of lateral heterogeneity ranges from <1–10 km in the San Fernando Valley, and from <6–20 km in the Los Angeles basin.

3.4. Case Study: Stress Orientation Heterogeneity Near the Newport-Inglewood Fault

Along the Newport-Inglewood fault within the west Los Angeles basin area, there are three boreholes within 300 m (coincident within borehole location uncertainty) of one another (BH #21–22 and 52) that have breakouts at three different depths (Figure 4). The basement in the area dips to the NE from 2 to 8 km depth, and almost all nearby earthquakes occur within the basement at depths >8 km, with an estimated FM SHmax of 18.2 ± 4.5 °EofN. The three nearly co-located boreholes result in distinct SHmax estimates that range from 41 ± 10 °WofN for the shallowest breakouts within 200 m of the surface to 18 ± 10 °EofN for the deepest breakouts at 3 km depth within 700 m of the sediment-basement interface. Intermediate depth breakouts at 2 km depth have an intermediate SHmax orientation of 9 ± 13 °WofN.
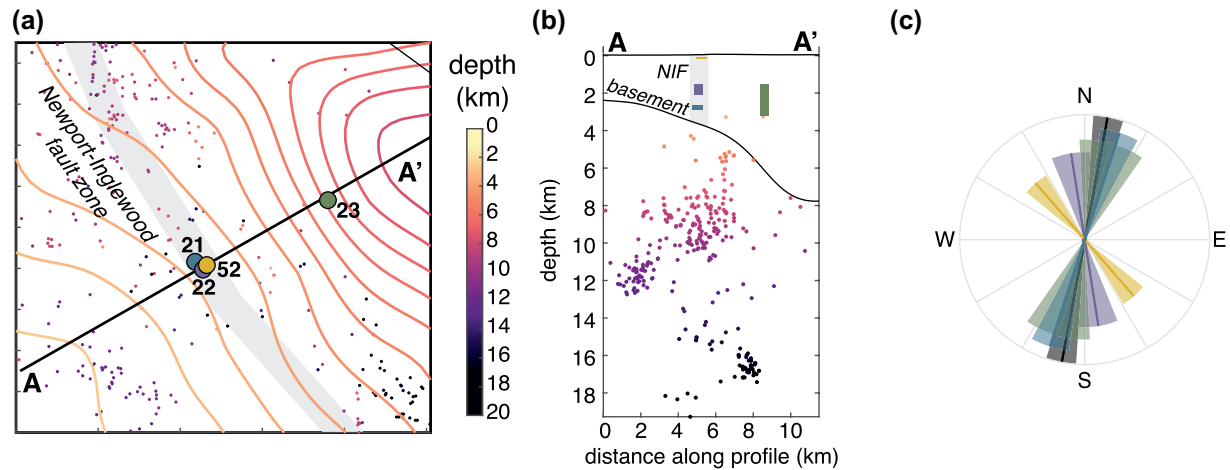
Figure 4. (a) Map view of BH #21, 22, 52, and 23 locations (blue, purple, yellow, and green circles, respectively), with earthquake locations (dots) and sediment-basement interface contours (lines) colored by depth. Gray shading indicates approximate surface trace of the Newport-Inglewood fault zone, and solid black line indicates profile. Map extent shown in Figure 1. (b) Cross section profile along A-A' showing the depth range of breakouts for each of the four boreholes (solid vertical lines) to scale. Surface topography and sediment-basement interface are indicated by black lines, and earthquakes shown in (a) are colored by depth. (c) SHmax estimates, with confidence intervals, for the four boreholes (colored lines and shading), along with SHmax estimate and 5–95% confidence interval range for earthquake focal mechanisms within 6 km of BH #21, of any depth (black line and shading). Line lengths are staggered to better visualize overlap.

The steady clockwise rotation of SHmax with depth along with the excellent fit between the deepest borehole breakouts and the earthquake focal mechanisms suggests significant stress heterogeneity with depth within the shallow crustal sediments, along with more homogeneous stress in and near the basement. This is in agreement with the observation from Section 3.3 that boreholes within the sedimentary basin with breakouts close to the sediment-basin interface are consistently well fit to the FM SHmax estimates. The next closest borehole (BH #23), 3.5 km to the northeast, contains breakouts from 1.5–3 km depth and has an estimated SHmax of 16 ± 19 °EofN, agreeing both with the FM SHmax estimates in the area and with the deepest breakouts from within the Newport-Inglewood fault zone, even though the basement depth in this area has dropped to 6 km. This suggests that the degree of stress orientation heterogeneity within the sediments decreases with sufficient distance from active locked faults, and that overall lateral heterogeneity is weaker than vertical heterogeneity.

4. Discussion

Figure 5 schematically illustrates a summary of the results described above. While region wide results indicate SHmax azimuth varies both with depth and laterally at length scales <10 km (Figure 3a), the geologic context subgroup results show that lateral heterogeneity is principally confined to the edges of sedimentary basins (Figures 3b and 3c). Depth heterogeneity is important both within (Figures 3e and 3f) and at the edges of (Figures 3b and 3c) basins, and stress state deep within the basins agrees well with the more homogeneous basement stress orientation (Figures 3d and 4). In areas of significant 3-D stress heterogeneity, depth variations are more prominent than lateral variations, evidenced by the lack of improved fit when earthquakes of any depth are considered (Figures 3b and 3c). That we see more heterogeneity in the basins versus the basement explains why BH orientations tend to be more heterogeneous (because they generally sample basins), while FM orientations are more homogeneous (because they generally sample basement). Within sediment basins, some depth heterogeneity may be captured by FMs when present (Figure 3e), but the persistent significant difference between FM
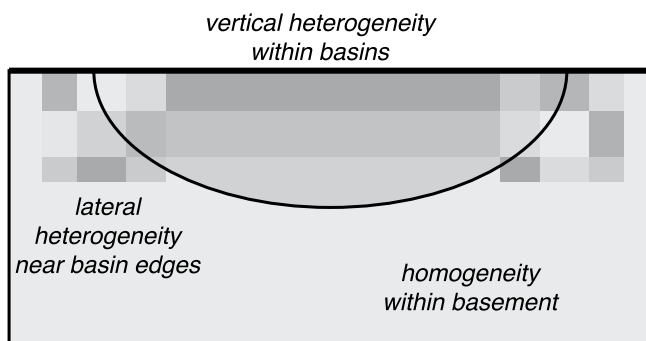

Figure 5. Schematic summary of results for stress orientation arrangements in the shallow crust. Solid black line represents sediment-basement interface.

and BH within the basins indicates the full heterogeneity must include scales smaller than those that were able to be explored with this earthquake distribution.

In this study, we did not use any time constraints, and instead simultaneously used the entire set of boreholes and earthquake catalog spanning at least four decades. This makes our analysis insensitive to any time-dependent changes in the stress field that may have occurred during that time, particularly in the vicinity of the 1994 M_w 6.7 Northridge earthquake in the San Fernando Valley (Hardebeck & Hauksson, 2001; Zhao et al., 1997), the aftershocks of which are abundant within the catalog. However, the similarity in behavior observed at the edges of the San Fernando Valley and Los Angeles basin makes us confident that our results are not being unduly biased by the abundance of Northridge aftershocks.

Previous studies of stress heterogeneity have focused on length scales both longer and shorter than those considered here, and in some cases obtained conflicting results. The World Stress Map project (Heidbach et al., 2018) used individual FMs and BH observations to analyze stress patterns globally and describe a smoothly varying field with large SHmax rotations across 40–60 km, while Persaud et al. (2020) performed new analysis of BH records and record substantial SHmax variation over lateral length scales <1 km. Wilde and Stock (1997) performed a regional analysis of BHs in the Los Angeles area to identify SHmax azimuths representing six subregions, with values varying by 60°. Yang and Hauksson (2013), on the other hand, used the methods of Hardebeck and Michael (2006) to invert the same FM catalog considered here for the 3-D deviatoric stress tensor orientation across southern California. At the 10–100 km scale they found similar SHmax variation as Wilde and Stock (1997), but with values in individual subregions differing by as much as 50° from those derived from BHs.

There have been similar levels of disagreement about the extent of SHmax variability with depth. Pierdominici and Heidbach (2012) compared shallow BHs and FMs versus deep FMs in smoothed stress fields across Italy. They found little SHmax variation between the shallowest 5 km and deeper crust, and conclude that lateral heterogeneity is more significant. In contrast, Schoenball and Davatzes (2017) studied BHs in eastern California and found significant SHmax variability with depth by corelating SHmax standard deviation with breakout length. In the vicinity of the Newport-Inglewood fault (Figure 4), Wilde and Stock (1997), who reported BH#22 and 52, noted their findings as an indication of significant depth variations in stress state, similar to those reported in the Cajon Pass borehole experiment (Shamir & Zoback, 1992). However, Mount and Suppe (1992), who reported BH #21 and 23, noted the broad agreement between these boreholes and estimates of FM SHmax available at the time (Hauksson, 1987), suggesting broad homogeneity in stress state.

The broad confusion in the literature about stress state heterogeneity in areas of active faulting demonstrates the utility of specifically examining stress heterogeneity at the intermediate length scales considered here. Taken together, the previous observations from the Los Angeles area (Mount & Suppe, 1992; Wilde & Stock, 1997; Yang & Hauksson, 2013) are in concert with the results presented in this study, of significant heterogeneity with depth, particularly in the vicinity of active faults and sediment basin margins, but of relative homogeneity within the sediment basins, and particularly within basement rock. We expect that these findings will be relevant to the interpretation of other regions, particularly those including active faults or sedimentary basin structures. However we note that while small-scale stress orientation heterogeneities are principally observed in active tectonic areas, studies distant from plate boundaries have demonstrated consistency between BH and FM stress observations (e.g., Gough & Bell, 1982; Lund Snee & Zoback, 2020).

Our analysis considers only heterogeneity in the SHmax direction, as SHmax is constrained by the borehole data. There may also be heterogeneity in the vertical stress, specifically variations in stress regime depending on which principal stress axis is most vertical. This potential heterogeneity can be addressed by focal mechanism studies, and in our study region the stress regime has been shown to vary laterally and with depth. The stress inferred from focal mechanisms in our study area exhibits both strike-slip and reverse regimes (Hardebeck & Hauksson, 2001; Yang & Hauksson, 2013), which Yang and Hauksson (2013) characterize as E-W trending bands of thrust faulting within the overall strike-slip regime of southern California. Two of these bands of thrust faulting encompass the deepest parts of the Los Angeles and Ventura Basins, with strike-slip regime in the western Transverse Ranges in between. The stress regime also varies with depth, transitioning to predominately reverse faulting at 10–15 km depth (Hardebeck & Hauksson, 2001). Yang and Hauksson (2011) found a similar change to a reverse regime at depth along the eastern margin

of the Los Angeles Basin, accompanied by a change in the SHmax direction. The aftershocks of the 1994 Northridge earthquake also vary from reverse faulting along the mainshock plane at depth to strike-slip faulting above in the hanging wall (Shearer et al., 2003). Variations in the plunge of the most-vertical stress axis with depth have been found in northern California (Bokelmann & Beroza, 2000) and in the San Jacinto Fault zone (Abolfathian et al., 2019), although a similar variation has not been reported in our study area.

One application of understanding crustal stress heterogeneity is the effective design of initial stress conditions for dynamic rupture simulations (Harris et al., 2018). Many of the geodynamic models that integrate multiple physical processes into estimates of lithosphere stress state rely heavily on observations of stress orientation from either FMs or BHs (Bird, 2017; Ghosh & Holt, 2012; Luttrell & Smith-Konter, 2017; Naliboff et al., 2012). The results presented above suggest that users of stress orientation observations should carefully consider the length scales of their problem of interest when deciding which indicators to adopt. If relying exclusively on FMs, considerable heterogeneity associated with sediment basins and near-fault processes may be overlooked. On the other hand, including BHs in a broader study may introduce unhelpful noise more relevant to individual fault segments than to a full plate boundary system.

In this work we have described stress orientation heterogeneity, but the magnitude and variation of stress magnitudes cannot be inferred from this analysis. Magnitude variations may exist in places of uniform orientation, or a stress field that rotates with depth may remain otherwise constant. One could potentially use the observed stress orientation heterogeneity described here as a constraint to infer stress magnitudes (e.g., Luttrell & Smith-Konter, 2017), but that is beyond the scope of the current investigation. Similarly, in this study we have focused on interpreting behavior that is broadly applicable across the region, but more might be learned about specific locations from comparison of the local FM inversions with individual BHs. A detailed description of each context is beyond the scope of this work, but the reader is directed to Supplementary Figures SB1–SB57 for the behavior of individual boreholes in their particular region of interest.

5. Conclusions

In conclusion, we have compared SHmax azimuths derived from published compilations of borehole breakouts with those derived from the inversion of local subsets of earthquake focal mechanisms in order to determine over what length scales and under what circumstances SHmax varies. We find strong evidence for depth variations in SHmax, particularly within sedimentary basins, but also evidence for a more homogeneous stress state within basement rock. Lateral variations in SHmax appear to be limited to the edges of sedimentary basins at length scales of <1–10 km in the San Fernando Valley and <6–20 km in the Los Angeles basin. The intermediate length scales considered here (1–35 km) push the lower-limit boundary of what can be resolved by focal mechanisms and effectively bridge the gap between previous BH and FM studies that found conflicting results with regard to stress heterogeneity.

Data Availability Statement

Focal mechanism data from 1981 to 2018 available from the Southern California Earthquake Data Center, https://scedc.caltech.edu/research-tools/alt-2011-yang-hauksson-shearer.html, last visited on January 8, 2020. Any use of trade, firm, or product names is for descriptive purposes only and does not imply endorsement by the U.S. Government.

References

Abolfathian, N., Martínez-Garzón, P., & Ben-Zion, Y. (2019). Spatiotemporal variations of stress and strain parameters in the San Jacinto fault zone. *Pure and Applied Geophysics*, *176*(3), 1145–1168. https://doi.org/10.1007/s00024-018-2055-y

Bird, P. (2017). Stress field models from Maxwell stress functions: Southern California. *Geophysical Journal International*, *210*, 951–963. https://doi.org/10.1093/gji/ggx207

Bokelmann, G. H., & Beroza, G. C. (2000). Depth-dependent earthquake focal mechanism orientation: Evidence for a weak zone in the lower crust. *Journal of Geophysical Research*, *105*(B9), 21683–21695. https://doi.org/10.1029/2000JB900205

Brudy, M., Zoback, M. D., Fuchs, K., Rummel, F., & Baumgärtner, J. (1997). Estimation of the complete stress tensor to 8 km depth in the KTB scientific drill holes: Implications for crustal strength. *Journal of Geophysical Research*, *102*(B8), 18453. https://doi.org/10.1029/96jb02942

Ghosh, A., & Holt, W. E. (2012). Plate motions and stresses from global dynamic models. *Science*, *335*(6070), 838–843. https://doi.org/10.1126/science.1214209

Gough, D. I., & Bell, J. S. (1982). Stress orientations from borehole wall fractures with examples from Colorado, east Texas, and northern Canada. *Canadian Journal of Earth Sciences*, *19*(7), 1358–1370. https://doi.org/10.1139/e82-118

Hardebeck, J. L., & Hauksson, E. (2001). Crustal stress field in southern California and its implications for fault mechanics. *Journal of Geophysical Research*, *106*(B10), 21859–21882. https://doi.org/10.1029/2001jb000292

Hardebeck, J. L., & Michael, A. J. (2006). Damped regional-scale stress inversions: Methodology and examples for southern California and the Coalinga aftershock sequence. *Journal of Geophysical Research*, *111*(B11), B11310. https://doi.org/10.1029/2005jb004144

Harris, R. A., Barall, M., Aagaard, B., Ma, S., Roten, D., Olsen, K., et al. (2018). A suite of exercises for verifying dynamic earthquake rupture codes. *Seismological Research Letters*, *89*(3). https://doi.org/10.1785/0220170222

Hauksson, E. (1987). Seismotectonics of the Newport-Inglewood fault zone in the Los Angeles basin, southern California. *Bulletin of the Seismological Society of America*, *77*(2), 539–561.

Hauksson, E., Yang, W., & Shearer, P. M. (2012). Waveform Relocated Earthquake Catalog for Southern California (1981 to 2011). *Bulletin of the Seismological Society of America*, *102*(5), 2239–2244. https://doi.org/10.1785/0120120010

Heidbach, O., Rajabi, M., Cui, X., Fuchs, K., Müller, B., Reinecker, J., et al. (2018). The World Stress Map database release 2016: Crustal stress pattern across T scales. *Tectonophysics*, *744*, 484–498. https://doi.org/10.1016/j.tecto.2018.07.007

Hickman, S., & Zoback, M. D. (2004). Stress orientations and magnitudes in the SAFOD pilot hole. *Geophysical Research Letters*, *31*(15), L15S12. https://doi.org/10.1029/2004gl020043

Kerkela, S., & Stock, J. (1996). Compression directions north of the San Fernando Valley determined from borehole breakouts. *Geophysical Research Letters*, *23*(23), 3365–3368. https://doi.org/10.1029/96GL03054

Lund Snee, J., & Zoback, M. D. (2020). Multiscale variations of the crustal stress field throughout North America. *Nature Communications*, *11*(1951). https://doi.org/10.1038/s41467-020-15841-5

Luttrell, K., & Smith-Konter, B. (2017). Limits on crustal differential stress in southern California from topography and earthquake focal mechanisms. *Geophysical Journal International*, *211*, 472–482. https://doi.org/10.1093/gji/ggx301

Mastin, L. (1988). Effect of borehole deviation on breakout orientations. *Journal of Geophysical Research*, *93*(B8), 9187–9195. https://doi.org/10.1029/JB093iB08p09187

Michael, A. J. (1984). Determination of stress from slip data: Faults and folds. *Journal of Geophysical Research*, *89*(B13), 11517. https://doi.org/10.1029/JB089iB13p11517

Michael, A. J. (1987). Use of focal mechanisms to determine stress: A control study. *Journal of Geophysical Research*, *92*(B1), 357–368. https://doi.org/10.1029/JB092iB01p00357

Mount, V., & Suppe, J. (1992). Present-day orientations adjacent to active strike-slip faults: California and Sumatra. *Journal of Geophysical Research*, *97*(B8), 11995–12013. https://doi.org/10.1029/92JB00130

Naliboff, J. B., Lithgow-Bertelloni, C., Ruff, L. J., & de Koker, N. (2012). The effects of lithospheric thickness and density structure on Earth's stress field. *Geophysical Journal International*, *188*, 1–17. https://doi.org/10.1111/j.1365-246X.2011.05248.x

Persaud, P., Pritchard, E. H., & Stock, J. (2020). Scales of stress heterogeneity near active faults in the Santa Barbara Channel, Southern California. *Geochemistry, Geophysics, Geosystems*, *21*, e2019GC008744. https://doi.org/10.1029/2019GC008744

Pierdominici, S., & Heidbach, O. (2012). Stress field of Italy—Mean stress orientation at different depths and wave-length of the stress pattern. *Tectonophysics*, *532–535*, 301–311. https://doi.org/10.1016/j.tecto.2012.02.018

Plumb, R., & Hickman, S. (1985). Stress-induced borehole elongation: A comparison between the four-arm dipmeter and the borehole televiewer in the Auburn Geothermal Well. *Journal of Geophysical Research*, *90*(B7), 5513–5521. https://doi.org/10.1029/JB090iB07p05513

Schoenball, M., & Davatzes, N. C. (2017). Quantifying the heterogeneity of the tectonic stress field using borehole data. *Journal of Geophysical Research*, *122*, 6737–6756. https://doi.org/10.1002/2017JB014370

Shamir, G., & Zoback, M. (1992). Stress orientation profile to 3.5 km depth near the San Andreas Fault at Cajon Pass, California. *Journal of Geophysical Research*, *97*(B4), 5059–5080. https://doi.org/10.1029/91JB02959

Shaw, J., Plesch, A., Tape, C., Suess, M. P., Jordan, T., Ely, G., et al. (2015). Unified Structural Representation of the southern California crust and upper mantle. *Earth and Planetary Science Letters*, *415*, 1–15. https://doi.org/10.1016/j.epsl.2015.01.016

Shearer, P. M., Hardebeck, J., Astiz, L., & Richards-Dinger, K. B. (2003). Analysis of similar event clusters in aftershocks of the 1994 Northridge, California, earthquake. *Journal of Geophysical Research*, *108*(B1), 2035. https://doi.org/10.1029/2001JB000685

Stock, J., & Healy, J. H. (1988). Continuation of a deep borehole stress measurement profile near the San Andreas Fault: 2. Hydraulic fracturing stress measurements at Black Butte, Mojave Desert, California. *Journal of Geophysical Research*, *93*(B12), 15196–15206. https://doi.org/10.1029/JB093iB12p15196

Vavryčuk, V. (2014). Iterative joint inversion for stress and fault orientations from focal mechanisms. *Geophysical Journal International*, *199*, 69–77. https://doi.org/10.1093/gji/ggu224

Wilde, M., & Stock, J. (1997). Compression directions in southern California (from Santa Barbara to Los Angeles Basin) obtained from borehole breakouts. *Journal of Geophysical Research*, *102*(B3), 4969. https://doi.org/10.1029/96jb03734

Yang, W., & Hauksson, E. (2011). The tectonic crustal stress field and style of faulting along the Pacific North America Plate boundary in Southern California. *Geophysical Journal International*, *194*(1), 100–117. https://doi.org/10.1785/0120100216

Yang, W., & Hauksson, E. (2013). The tectonic crustal stress field and style of faulting along the Pacific North America Plate boundary in Southern California. *Geophysical Journal International*, *194*(1), 100–117. https://doi.org/10.1093/gji/ggt113

Yang, W., Hauksson, E., & Shearer, P. M. (2012). Computing a large refined catalog of focal mechanisms for Southern California (1981-2010): Temporal stability of the style of faulting. *Bulletin of the Seismological Society of America*, *102*(3), 1179–1194. https://doi.org/10.1785/0120110311

Zajac, B., & Stock, J. (1997). Using borehole breakouts to constrain the complete stress tensor: Results from the Sijan Deep Drilling Project and offshore Santa Maria Basin, California. *Journal of Geophysical Research*, *102*(B5), 10083. https://doi.org/10.1029/96jb03914

Zhao, D., Kanamori, H., & Wiens, D. (1997). State of stress before and after the 1994 Northridge earthquake. *Geophysical Research Letters*, *24*(5), 519–522. https://doi.org/10.1029/97GL00258

Zoback, M. D., & Healy, J. H. (1992). In situ stress measurements to 3.5 km depth in the Cajon Pass Scientific Research Borehole: Implications for the mechanics of crustal faulting. *Journal of Geophysical Research*, *97*(B4), 5039. https://doi.org/10.1029/91jb02175

Zoback, M. D., Hickman, S., & Ellsworth, W. (2010). Scientific drilling into the San Andreas Fault Zone. *Eos Transactions AGU*, *91*(22), 197–199. https://doi.org/10.1029/2010EO220001